Cell Stem Cell
Article

Directly Reprogrammed Fibroblasts Show Global Epigenetic Remodeling and Widespread Tissue Contribution

Nimet Maherali,[1,2,6] Rupa Sridharan,[3,6] Wei Xie,[3] Jochen Utikal,[1] Sarah Eminli,[1] Katrin Arnold,[1] Matthias Stadtfeld,[1] Robin Yachechko,[3] Jason Tchieu,[3] Rudolf Jaenisch,[5] Kathrin Plath,[3,4,*] and Konrad Hochedlinger[1,*]

[1] Massachusetts General Hospital Cancer Center and Center for Regenerative Medicine, Harvard Stem Cell Institute, 185 Cambridge Street, Boston, MA 02114, USA
[2] Department of Molecular and Cellular Biology, Harvard University, 7 Divinity Avenue, Cambridge, MA 02138, USA
[3] Department of Biological Chemistry
[4] Molecular Biology Institute
Johnson Comprehensive Cancer Center and Institute for Stem Cell Biology and Medicine, UCLA School of Medicine, Los Angeles, CA 90095, USA
[5] Whitehead Institute and Department of Biology, Massachusetts Institute of Technology, 9 Cambridge Center, Cambridge, MA 02142, USA
[6] These authors contributed equally to this work.
*Correspondence: kplath@mednet.ucla.edu (K.P.), khochedlinger@helix.mgh.harvard.edu (K.H.)
DOI 10.1016/j.stem.2007.05.014

SUMMARY

Ectopic expression of the four transcription factors Oct4, Sox2, c-Myc, and Klf4 is sufficient to confer a pluripotent state upon the fibroblast genome, generating induced pluripotent stem (iPS) cells. It remains unknown if nuclear reprogramming induced by these four factors globally resets epigenetic differences between differentiated and pluripotent cells. Here, using novel selection approaches, we have generated iPS cells from fibroblasts to characterize their epigenetic state. Female iPS cells showed reactivation of a somatically silenced X chromosome and underwent random X inactivation upon differentiation. Genome-wide analysis of two key histone modifications indicated that iPS cells are highly similar to ES cells. Consistent with these observations, iPS cells gave rise to viable high-degree chimeras with contribution to the germline. These data show that transcription factor-induced reprogramming leads to the global reversion of the somatic epigenome into an ES-like state. Our results provide a paradigm for studying the epigenetic modifications that accompany nuclear reprogramming and suggest that abnormal epigenetic reprogramming does not pose a problem for the potential therapeutic applications of iPS cells.

INTRODUCTION

Reprogramming of cells by nuclear transfer (Wakayama et al., 1998; Wilmut et al., 1997) and cell fusion (Cowan et al., 2005; Tada et al., 2001) allows for the re-establishment of a pluripotent state in a somatic nucleus (Hochedlinger and Jaenisch, 2006). Although the molecular mechanisms of nuclear reprogramming remain elusive, cell-fusion experiments have implied that reprogramming factors can be identified in ES cells and be used to directly induce reprogramming in somatic cells. Indeed, a rational approach recently led to the identification of four transcription factors whose expression enabled the induction of a pluripotent state in adult fibroblasts (Takahashi and Yamanaka, 2006). Yamanaka and colleagues demonstrated that retroviral expression of the transcription factors Oct4, Sox2, c-Myc, and Klf4, combined with genetic selection for Fbx15 expression, gives rise to iPS cells directly from fibroblast cultures. Fbx15-selected iPS cells contributed to diverse tissues in midgestation embryos; however, these embryos succumbed at midgestation, indicating a restricted developmental potential of iPS cells compared with ES cells. Consistent with this observation, only part of the ES cell transcriptome was expressed in iPS cells, and methylation analyses of the chromatin state of the Oct4 and Nanog promoters demonstrated an epigenetic pattern that was intermediate between that of fibroblasts and ES cells.

These observations raised three fundamental questions about the molecular and functional nature of directly reprogrammed cells: (1) can selection for a gene that is essential for the ES cell state generate pluripotent cells that are more similar to ES cells than the previously described Fbx15-selected iPS cells; (2) does the pluripotent state of iPS cells depend on continuous expression of exogenous factors; and (3) does transcription factor-induced reprogramming reset the epigenetic landscape of a fibroblast genome into that of a pluripotent cell.

Successful reprogramming of somatic cells by nuclear transfer or cell fusion is thought to require faithful remodeling of epigenetic modifications such as DNA methylation,

histone modifications, and reactivation of a silent X chromosome in female cells (Rideout et al., 2001). Aberrant epigenetic reprogramming is assumed to be the principal reason for the developmental failure and abnormalities seen in animals cloned by nuclear transfer. Thus, the question of epigenetic reprogramming is of particular relevance for the potential therapeutic applications of iPS cells, as epigenetic aberrations can result in pathological conditions such as cancer (Gaudet et al., 2003).

Here, we have generated iPS cells from fibroblasts by using novel selection approaches and assessed their epigenetic status at a gene-specific, chromosome-wide, and genome-wide level. Our results demonstrate that the ectopic expression of four transcription factors is sufficient to globally reset the epigenetic state of fibroblasts into that of pluripotent cells that are remarkably similar to ES cells.

RESULTS

Generation of iPS Cells Using Nanog-Selectable Fibroblasts

We retrovirally infected female mouse embryonic fibroblasts (MEFs) carrying a GFP-IRES-puro cassette in the endogenous Nanog locus, referred to as Nanog-GFP (Hatano et al., 2005), with cDNAs encoding *Oct4*, *Sox2*, *c-MYC* (T58A mutant, which stabilizes the protein) (Sears et al., 2000), and *Klf4*. In contrast to the previously reported Fbx15 selection, which was applied 3 days after infection (Takahashi and Yamanaka, 2006), selection for Nanog expression at 3 days postinfection resulted in no colonies, suggesting different reactivation kinetics of the Fbx15 and Nanog genes. When selection was applied 7 or more days after infection, resistant colonies reproducibly emerged. Of the five lines that were expanded (Table S1 in the Supplemental Data available with this article online), two lines maintained homogeneous cultures that looked identical to ES cells and expressed the ES cell surface markers SSEA1 and CD9 (data not shown). In contrast, the other three clones gave rise to heterogeneous cultures after multiple passages, which contained both an ES-like population and a separate population of small round, rapidly dividing cells. FACS sorting for Nanog-GFP, SSEA-1, and CD9, followed by subcloning, was sufficient to eliminate these round cells, suggesting that this population was distinct from the ES-like cells. Interestingly, the onset of selection for the two homogeneous cell lines occurred at 3 weeks postinfection, whereas the heterogeneous lines had undergone selection at 1 week postinfection, suggesting that delayed selection may be advantageous for obtaining a more pure population of iPS cells.

We focused our subsequent studies on the homogeneous ES-like cell line 2D4 and the re-sorted and subcloned line 1A2, which we will refer to as iPS cells. Southern blot analysis of retroviral integration sites revealed the presence of all four retrovirally encoded genes in both iPS lines, and a test for genomic imprinting confirmed that the iPS cells were not derived from rare primordial germ cells that may have been present in the fibroblast culture (Figure S1). In contrast to Fbx15-selected iPS cells (Takahashi and Yamanaka, 2006), Nanog-selectable iPS cells exhibited feeder-independent growth, as they maintained an ES-like morphology, Nanog expression, and alkaline phosphatase (AP) activity in the absence of feeders and puromycin selection (Figures 1A and 1B). Withdrawal of LIF resulted in the expected differentiation into GATA-4-expressing cells resembling primitive endoderm (Figure 1B and Figure S2A), and differentiation was accompanied by a loss of Nanog expression (Figure S2B). RT-PCR analysis indicated expression of Oct4 and Sox2 from the endogenous loci, along with the other ES cell markers Nanog, ERas, and Cripto (Figure 1C). Protein levels for Oct4, Sox2, c-Myc, and Klf4 were similar between iPS cells and control ES cells (Figure 1D), and immunofluorescence showed that Oct4 and Sox2 were efficiently downregulated upon retinoic acid-induced differentiation, demonstrating that the virally encoded transcription factor genes remained effectively silenced in differentiated cells (Figure S3). Quantitative PCR analysis for the four retrovirally expressed genes showed strong expression in fibroblasts infected with the individual retroviruses but efficient silencing in homogenous iPS cells (Figure 1E). Injection of 2D4 iPS cells into SCID mice gave rise to teratomas containing cell types representative of the three germlayers, confirming their pluripotency (Figure 1F). These data suggested that retrovirally expressed *Oct4*, *Sox2*, *c-MYC*, and *Klf4*, in combination with selection for Nanog reactivation, can yield iPS cells that share many properties with ES cells.

Nanog-Selectable iPS Cells Confer an ES Cell-like Phenotype upon Somatic Cells

To determine whether Nanog-selectable iPS cells possess functional attributes similar to ES cells, we tested their ability to impose an ES-like phenotype upon somatic cells in the context of cell fusion. We fused cells from the puromycin-resistant 2D4 iPS cell line with hygromycin-resistant MEFs (Figure 2A). Two weeks after fusion, we recovered seven double-resistant tetraploid hybrid clones that had an ES cell-like morphology and continued to express Nanog-GFP (Figures 2B and 2C). One hybrid colony was recovered when control Nanog-GFP ES cells were fused with hygromycin-resistant MEFs. To test pluripotency, hybrid cells were injected into immunocompromised mice; after 4 weeks, teratomas containing cell types representative of all three germ layers were isolated (data not shown).

To directly test for reprogramming of the somatic cell genome, we took advantage of an endogenous Oct4 selection allele (Oct4-Neo) contained in the MEFs in addition to the constitutive hygromycin resistance marker. No clones could be obtained if G418 was used in the initial selection process, suggesting that the reprogramming of the somatic cell Oct4 locus, like that of the endogenous Nanog locus, is a gradual process. We therefore expanded puromycin/hygromycin-resistant hybrids before subjecting them to puromycin/G418 selection to test for

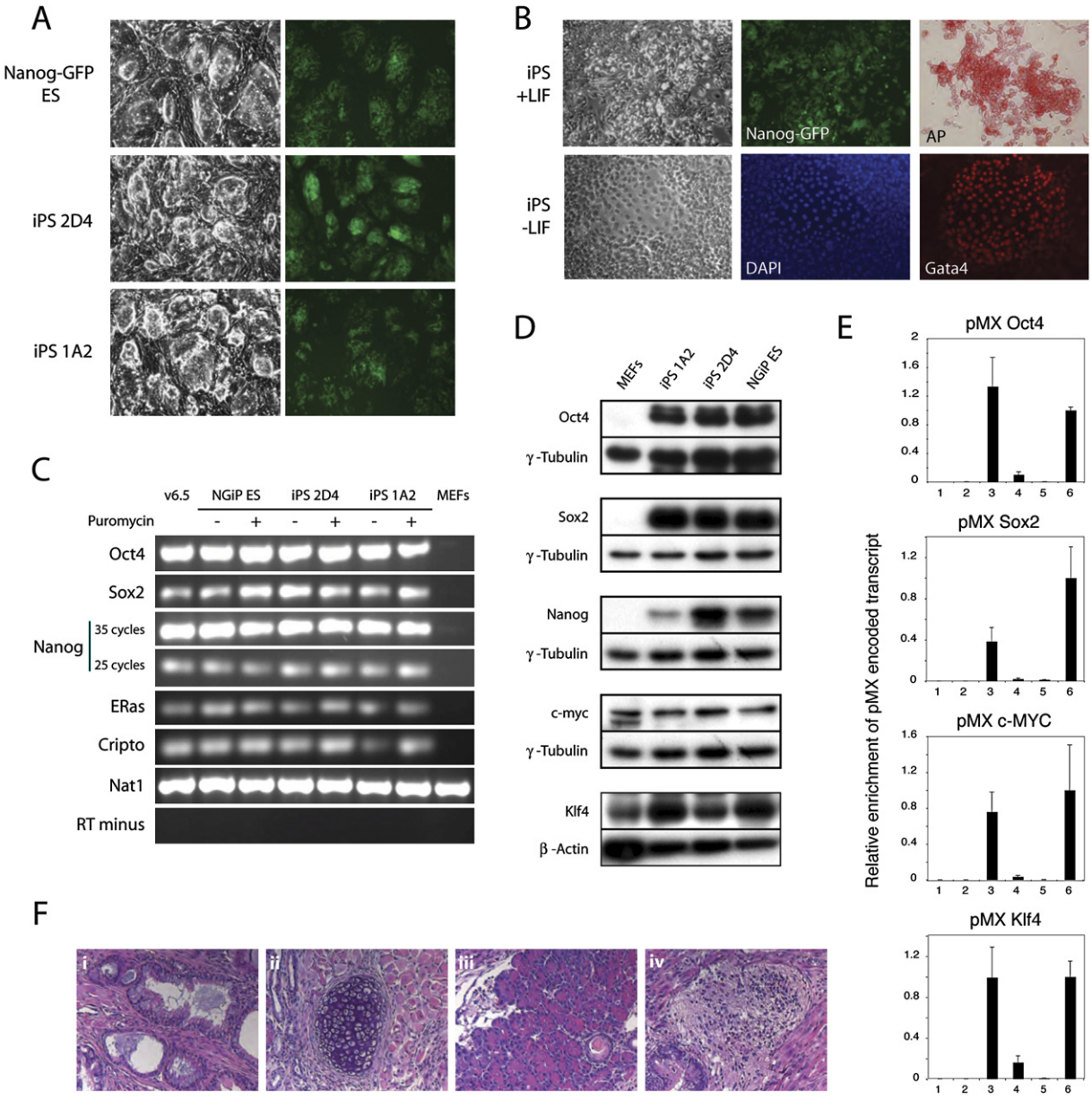

Figure 1. ES Cell-like Properties of Nanog-Selected iPS Cells

(A) Morphology and Nanog promoter-driven GFP expression in ES cells (Nanog-GFP ES) and two iPS cell lines grown on feeders in the absence of puromycin selection.

(B) Effect of LIF withdrawal on iPS cells. Cells were grown for three passages without feeders. In the presence of LIF, 2D4 iPS cells maintain an ES-like morphology, express endogenous Nanog as indicated by GFP expression, and are alkaline phosphatase (AP) positive. Upon LIF withdrawal, iPS cells upregulate the primitive endoderm marker Gata4 as detected by immunostaining. A phase contrast image and counterstaining of the same cells with DAPI is shown.

(C) RT-PCR analysis of ES cell marker gene expression in Nanog-GFP (NGiP) ES cells, and two iPS cell lines grown with and without continued puromycin selection, as well as in wild-type ES cells (V6.5) and MEFs as additional reference points. Primers for Oct4 and Sox2 are specific for transcripts from the respective endogenous locus. Nat1 was used as a loading control.

(D) Western blot analysis for expression of Nanog, Oct4, Sox2, c-*myc*, and Klf4 in iPS cell lines, MEFs, and Nanog-GFP (NGiP) ES cells. Anti-tubulin and anti-actin antibodies were used to control for loading.

(E) Quantitative PCR analysis of pMX retroviral transcription in (1) wild-type MEFs, (2) wild-type ES cells, (3) cells from the heterogeneous iPS line 1A2 before sorting and subcloning, (4) 1D4 iPS, (5) 2D4 iPS, and (6) MEFs infected with the respective pMX virus. Transcript levels were normalized to β-actin. It should be noted that the retroviruses in the 2D4 iPS line appear completely silenced, whereas the heterogeneous 1A2 line still shows abundant expression of the exogenous factors. Error bars represent the standard deviation of triplicate reactions.

(F) Teratoma derived from iPS line 1A2 showing differentiation into cell types from all three germ layers: epithelial structures (i), cartilage with surrounding muscle (ii), glandular structures (iii), and neural tissue (iv).

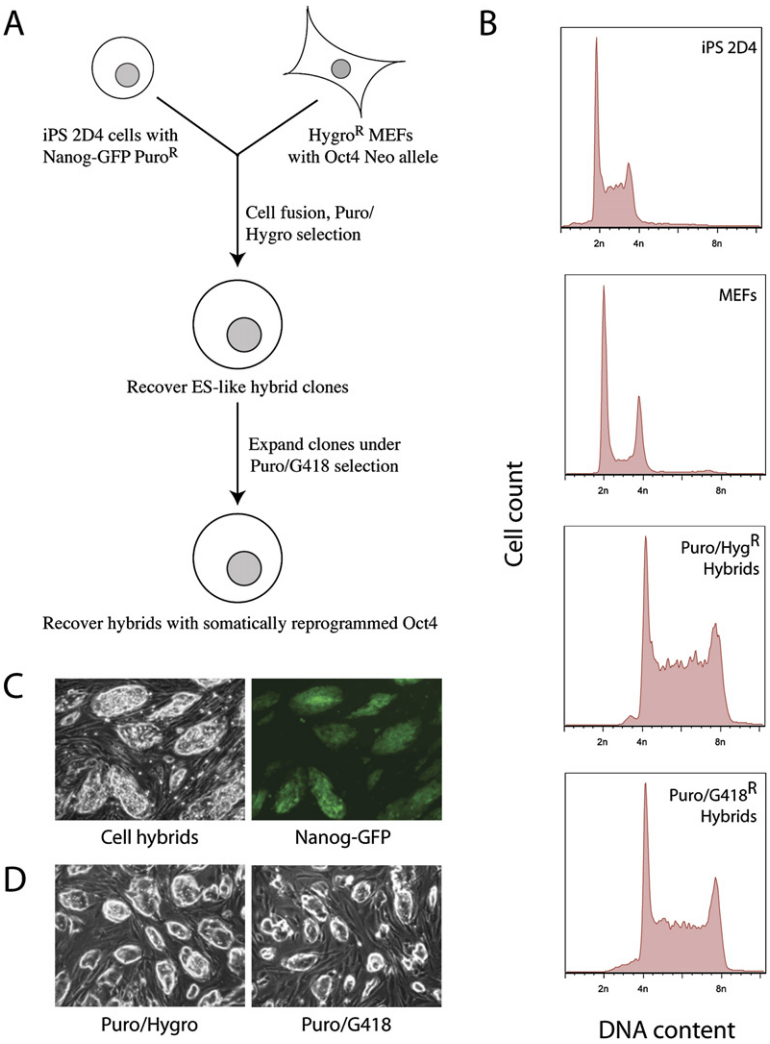

Figure 2. Fusion of iPS Cells with Somatic Cells

(A) Schematic of cell fusion between 2D4 iPS cells and hygromycin-resistant MEFs that carry an Oct4-Neo-selectable allele.

(B) DNA content analysis of 2D4 iPS cells, MEFs, and 2D4/MEF cell hybrids maintained either under puromycin/hygromycin selection or puromycin/G418 selection.

(C) Phase contrast image showing ES-like morphology of cell hybrids under puromycin/hygromycin selection. Expression of GFP from the Nanog locus in 2D4 iPS cells is continued in hybrids.

(D) Comparison of puromycin/hygromycin and puromycin/G418 selection in hybrids. Cells are viable and maintain ES-like morphology under both conditions.

reactivation of the somatic Oct4 gene. All puromycin/hygromycin-resistant colonies were viable under puromycin/G418 selection, indicating that the somatic genome had been reprogrammed at the endogenous Oct4 locus (Figure 2D). These results show that Nanog-selected iPS cells, similar to ES cells, carry reprogramming activity and can confer an ES-like state upon a somatic cell genome.

Ectopic Oct4 Expression Is Dispensable for the Maintenance of iPS Cells

Fbx15-selected iPS cells showed persistent retroviral expression of Oct4 and Sox2 with negligible expression from the respective endogenous loci, suggesting a continuous requirement for the exogenously provided factors to maintain the self-renewal and pluripotency of iPS cells (Takahashi and Yamanaka, 2006). To corroborate our gene expression data that suggested efficient retroviral gene silencing in iPS cells, we decided to genetically test whether continuous Oct4 expression is required for the maintenance of iPS cells by using fibroblasts carrying a doxycycline-inducible Oct4 transgene in their genome (Hochedlinger et al., 2005) (Figure 3A).

To initially determine whether colonies could be obtained by using the Oct4 inducible system, we infected Oct4-inducible MEFs with Sox2, c-MYC, and Klf4 retroviruses without any selection. In the absence of doxycycline, no AP-positive colonies were recovered, whereas in the presence of doxycycline, several hundred AP-positive colonies emerged, indicating a strict dependence on transgenic Oct4 expression for the establishment of AP-positive colonies (Figure 3B). Subsequently, iPS cells were generated from tail tip fibroblasts (TTFs) carrying both the Oct4-inducible allele and the Oct4-Neo allele to verify the reprogrammed state of resultant cells (Figure 3A). Target cells were infected with Sox2, c-MYC, and Klf4 in the presence of doxycycline. Based on our previous observation that a late onset of drug selection was advantageous, we attempted to establish iPS colonies based solely on ES cell-like morphology without initial selection. Forty-eight individual ES-like colonies were picked at 3 weeks postinfection, two

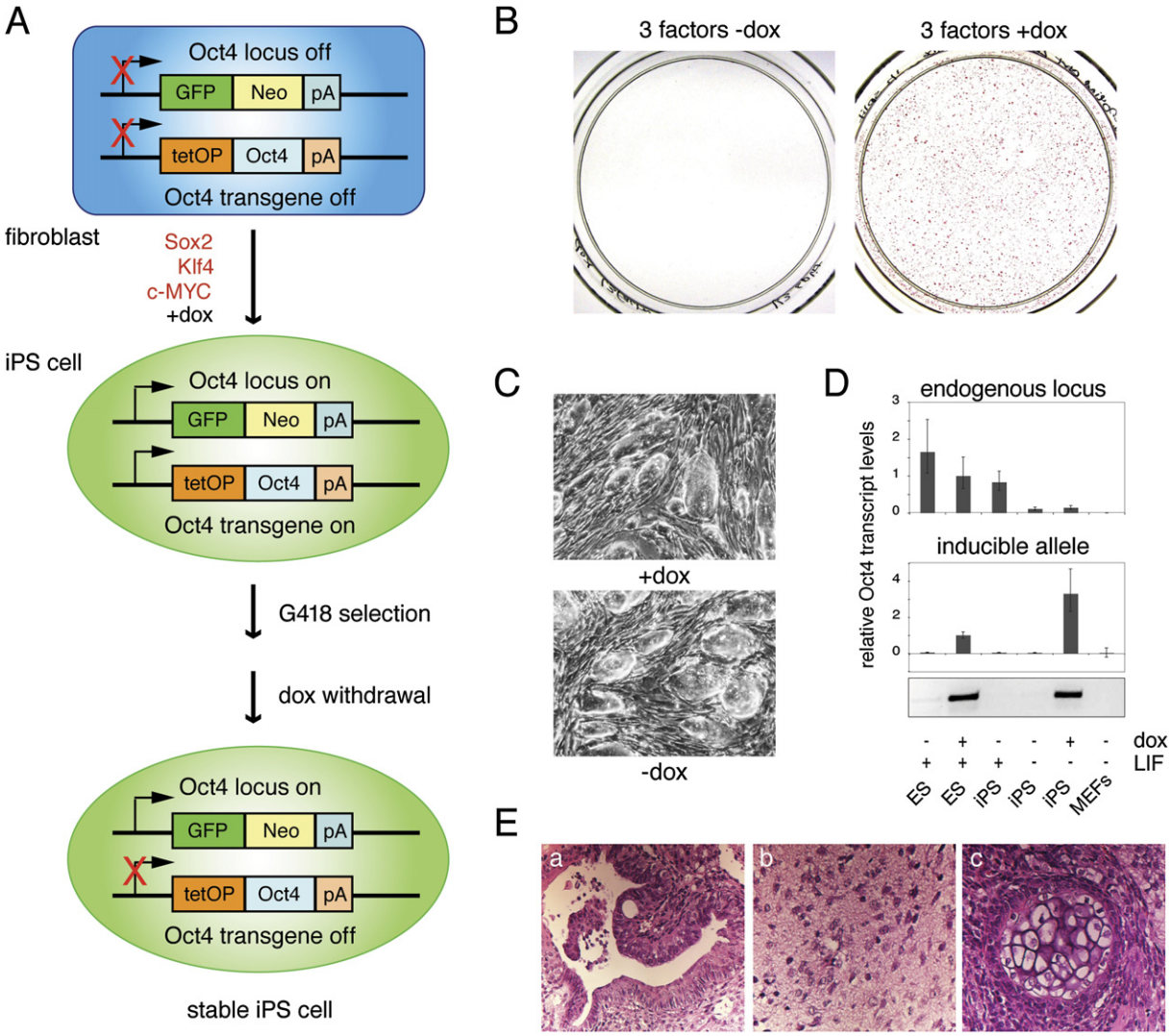

Figure 3. Requirement for Exogenous Oct4 for the Maintenance of iPS Cells

(A) Schematic of iPS cell generation with Oct4-inducible fibroblasts.

(B) MEFs infected with Sox2, c-MYC, and Klf4, in the absence or presence of doxycycline-inducible Oct4 expression. Shown are plates stained for alkaline phosphatase activity.

(C) Morphology of Oct4-inducible Oct4-selectable (Oct4-Neo) iPS cells after three passages grown in G418 in the absence or presence of doxycycline.

(D) Quantitative PCR analysis of Oct4 levels in Oct4-inducible iPS cells. Levels of transcripts from the endogenous and inducible alleles were measured in undifferentiated iPS cells (+LIF, −dox), differentiated iPS cells (−LIF, −dox), and differentiated iPS cells reinduced at 5 days after LIF withdrawal (−LIF, +dox). Transcript levels were normalized to β-actin. ES cells carrying the inducible Oct4 allele and wild-type MEFs served as controls. Error bars represent the standard deviation of triplicate reactions.

(E) Pluripotency demonstrated by teratoma formation. Tumors were generated by using Oct4-inducible iPS cells that had been passaged five times in the absence of doxycycline. Shown are epithelial structures (endodermal [a]), neural tissue (ectodermal [b]), and cartilage (mesodermal [c]).

of which grew into stable ES cell-like lines in the continued presence of doxycycline and G418. Both cell lines survived under G418 selection, indicating that the endogenous Oct4 gene had been reactivated and iPS cells had been generated. Importantly, when doxycycline was withdrawn from the media, these cells could be passaged many times in the presence of G418 without changes in their growth behavior or morphology (Figure 3C). To exclude the possibility of viral insertion and aberrant Oct4 transgene activation in the absence of doxycycline, quantitative PCR analysis of endogenous and induced Oct4 expression was performed to analyze expression levels during differentiation and induction (Figure 3D). Undifferentiated iPS cells showed high levels of endogenous Oct4 expression and complete absence of transgene expression. Oct4 levels declined in the absence of LIF and reappeared upon administration of doxycycline, indicating

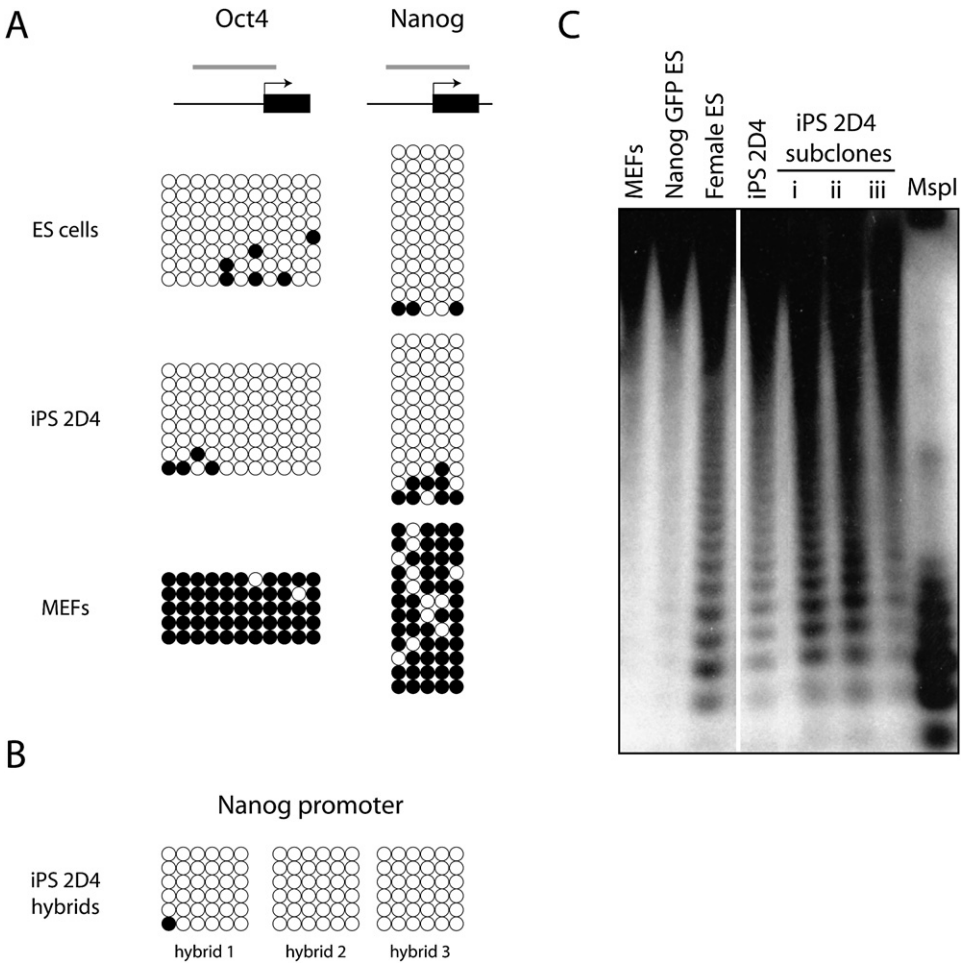

Figure 4. Gene-Specific and Global DNA Methylation Status in iPS Cells

(A) Bisulfite sequencing of the Oct4 and Nanog promoter regions in ES cells, 2D4 iPS cells, and MEFs. Promoter regions containing the differentially methylated CpGs are shown with respect to the transcriptional start site (arrow). Open circles represent unmethylated CpGs; closed circles denote methylated CpGs.

(B) Bisulfite sequencing of the Nanog promoter in cell hybrids generated through fusion of iPS 2D4 cells and MEFs. Data shown for puromycin/hygromycin-resistant hybrids as in Figure 2.

(C) Southern blot analysis of global DNA methylation using a satellite repeat probe. Genomic DNA from MEFs, male Nanog-GFP ES cells, female ES cells, iPS 2D4 cells, and three subclones was digested with the methylation-sensitive restriction enzyme HpaII and hybridized with a minor satellite repeat probe. Male ES cell DNA digested with the nonmethylation-sensitive isoschizomer MspI served as a control. Lower molecular weight bands are indicative of hypomethylation.

differentiation-dependent downregulation of endogenous Oct4 expression and sustained responsiveness of cells to doxycycline, respectively (Figure 3D). The ability to form well-differentiated teratomas demonstrated the pluripotency of these cells (Figure 3E). We conclude that the endogenous Oct4 locus had been sufficiently reprogrammed by the four transcription factors to maintain iPS cells in a pluripotent state in the absence of exogenous Oct4 expression.

Gene-Specific and Global DNA Methylation Is Similar between iPS Cells and ES Cells

Based on the ES cell-like properties of reprogrammed fibroblasts, we wondered if iPS cells had acquired an epigenetic state similar to ES cells. Reprogramming of a somatic genome by nuclear transfer or cell fusion is accompanied by epigenetic changes such as DNA demethylation of pluripotency genes at their promoter regions (Cowan et al., 2005; Tada et al., 2001). We used bisulfite sequencing to assess the methylation status of the Oct4 and Nanog promoters, which had previously been shown to be incompletely demethylated in Fbx15-selected iPS cells (Takahashi and Yamanaka, 2006). Both promoter elements, which were methylated in MEFs, showed demethylation in Nanog-selected iPS cells and ES cells, suggesting proper epigenetic reprogramming of these two pluripotency genes (Figure 4A). Furthermore, demethylation of the Nanog promoter occurred in cell

hybrids generated through fusion of iPS cells and MEFs (Figure 4B; refer to Figure 2), confirming that iPS cells harbor reprogramming activity and can induce epigenetic changes in differentiated cells.

Female ES cells, in contrast to male ES cells and differentiated cells, show global DNA hypomethylation of the genome, which is attributable to the presence of two active X chromosomes (Xa) (Zvetkova et al., 2005). Using a methylation-sensitive restriction enzyme assay, we detected global hypomethylation of minor satellite repeats in the 2D4 iPS cell line, similar to female control ES cells (Figure 4C). These results suggest that iPS cells have obtained an epigenetic state similar to that of female ES cells.

Dynamics of X Inactivation in Female Nanog-Selectable iPS Cells

Global DNA hypomethylation in iPS cells suggested that the inactive X chromosome (Xi) is reactivated in female iPS cells. To directly test this hypothesis, we asked if X chromosome reactivation occurs during the generation of iPS cells. X inactivation is one of the most dramatic examples of heterochromatin formation in mammalian cells and is regulated by two noncoding RNAs, *Xist* and its antisense transcript *Tsix*, which are reciprocally expressed (Thorvaldsen et al., 2006). Undifferentiated female ES cells carry two Xa and express *Tsix* from both X chromosomes to repress *Xist* expression. Upon differentiation, *Xist* becomes strongly upregulated on the future Xi to induce silencing, whereas *Tsix* disappears and is absent in somatic cells. The *Xite* locus, a third locus important for X inactivation located downstream of *Tsix*, is expressed in a *Tsix*-like pattern (Ogawa and Lee, 2003).

We first assessed the X inactivation status in female Nanog-GFP MEFs by using fluorescence in situ hybridization (FISH) to analyze *Xist* and *Tsix* RNA and X-linked gene expression. In agreement with the presence of an Xi, 96% of the fibroblasts carried an *Xist* RNA-coated X chromosome and showed expression of the *pgk1* gene from the other X chromosome (Figures 5A–5C). The 2D4 iPS cell line showed a pattern of *Xist*, *Tsix*, and *pgk1* expression highly reminiscent of undifferentiated ES cells (Figures 5A–5C). That is, *Tsix* and *pgk1* were expressed biallelically at high levels, and *Xist* RNA could not be detected, demonstrating the presence of two Xa. In addition, RT-PCR analysis detected transcripts from the *Xite* locus in both ES cells and 2D4 iPS cells, but not in the parental fibroblast population (Figure 5D).

Upon initiation of X inactivation, characteristic chromatin modifications are imposed on the future Xi that ensure stable silencing of the chromosome (Heard, 2005; Ng et al., 2007). We used immunofluorescence to analyze the presence of Xi-linked chromatin modifications in iPS cells. Female Nanog-GFP MEFs showed the expected frequencies of the Xi-like enrichment for histone H3 trimethylated at lysine 27, histone H4 lysine 20 monomethylation, and for the Polycomb group (PcG) protein Ezh2, which is responsible for mediating H3K27 trimethylation. In contrast, iPS cells, like ES cells, showed abundant and uniform nuclear staining for these chromatin marks with no Xi-like enrichment (Figure 5E). Together, these data indicate that four transcription factors, in combination with Nanog selection, are sufficient to induce transcriptional reactivation of the Xi, to reset the expression patterns of the three noncoding transcripts essential for regulation of X inactivation, and to erase the chromatin modifications that are specific to the Xi.

Next, we tested if 2D4 iPS cells could undergo X inactivation upon differentiation. Consistent with the ability of iPS cells to silence one of their X's, we detected an *Xist* RNA-coated chromosome in 2D4 iPS cells undergoing retinoic acid-induced differentiation (Figure 5F). The *Xist*-coated chromosome showed no overlap with RNA polymerase II in agreement with a silent state of that X (Figure 5G). Furthermore, similar to differentiating female ES cells, the *Xist* RNA-coated X chromosome in iPS cells was almost always coincident with a region of enrichment of H3me3K27 and its methyltransferase Ezh2 upon initiation of X inactivation (Figure 5H). The coincidence of Ezh2 accumulation and H3me3K27 enrichment on the Xi are hallmarks only of early phases of X inactivation (Plath et al., 2003; Silva et al., 2003). We concluded that X chromosome inactivation in female iPS cells displays the same dynamics as in female ES cells.

Random X Inactivation in Differentiating iPS Cells

X chromosome inactivation occurs nonrandomly in the extraembryonic lineages and in early preimplantation embryos, whereas it is random in the epiblast and differentiating ES cells. Analysis of X inactivation in cloned mouse embryos has shown that the somatic Xi is reprogrammed during nuclear transfer to enable random X inactivation in embryonic cells while the memory of the Xi is maintained in extraembryonic tissues where it replaces the gametic imprint (Eggan et al., 2000). We therefore tested whether transcription factor-induced reprogramming can erase the memory of the somatically inactivated Xi, thus enabling random X inactivation in differentiating iPS cells. Because we were unable to distinguish between the two X chromosomes in Nanog-selectable 2D4 iPS cells, we generated iPS cells from female fibroblasts carrying an X-linked reporter transgene (X^{GFP}) with a cytomegalovirus promoter driving expression of green fluorescent protein (GFP) (Hadjantonakis et al., 1998) (Figure 6A). This reporter is subject to silencing by X inactivation and thus allowed us to determine which X chromosome is silenced in differentiating iPS cells. TTFs were isolated from a female mouse heterozygous for the GFP transgene and carrying the Oct4-Neo allele. Consistent with random X inactivation in the fibroblast population, 34% of the TTF cells were GFP positive (Xa^{GFP}/Xi) and 66% of the cells were GFP negative (Xi^{GFP}/Xa) (Figures 6A and 6B). Some skewing of X inactivation was expected and likely reflected differences in the genetic backgrounds of the two X chromosomes. GFP-negative cells isolated by two rounds of FACS sorting were infected with the retroviruses encoding the four transcription factors, and resulting ES-like colonies were screened for reactivation of the Xi^{GFP} based on GFP re-expression. Four entirely green colonies were

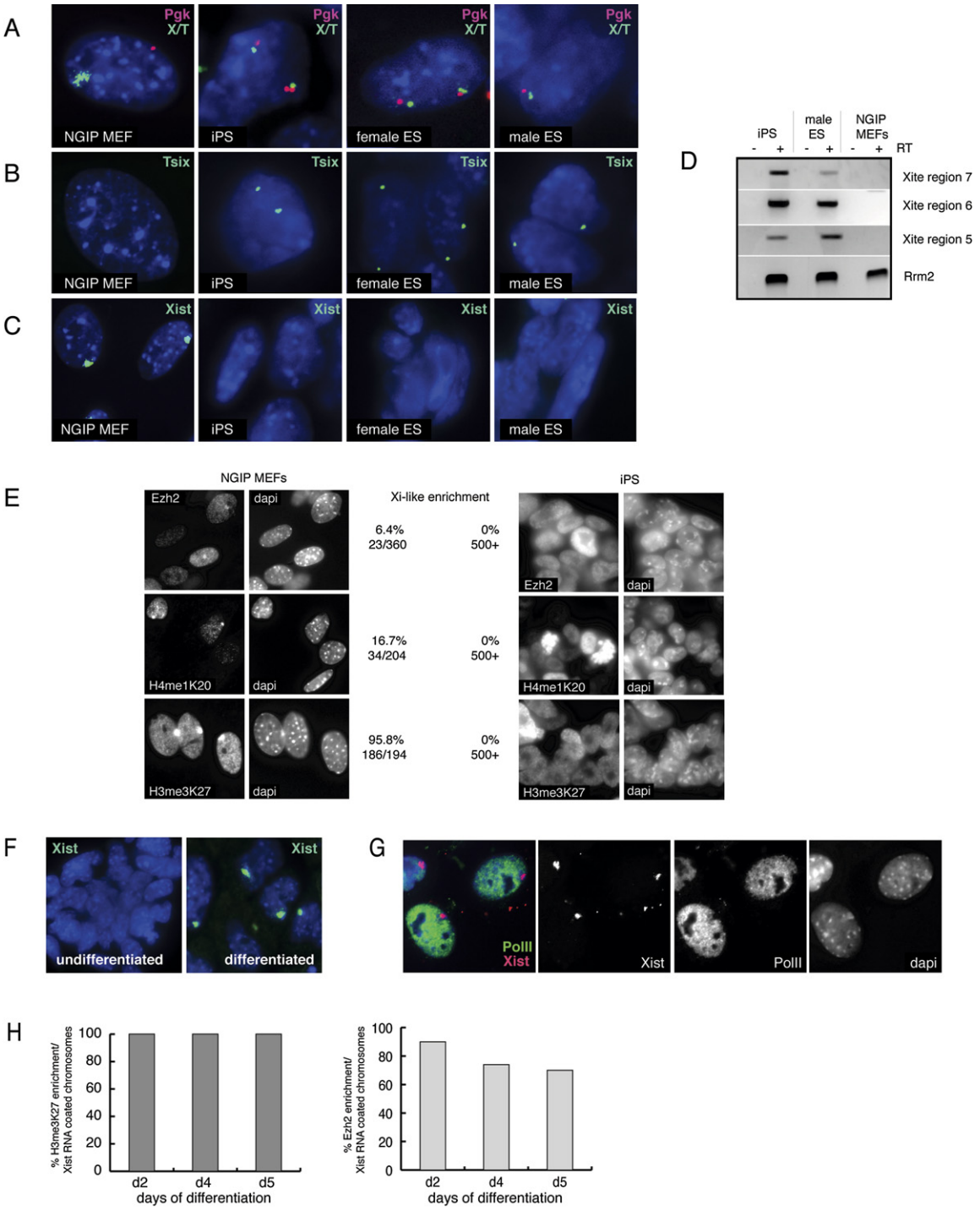

Figure 5. X Chromosome Dynamics in iPS Cells

(A) Localization and expression of *Xist*, *Tsix*, and *pgk1* RNA in the nuclei of female Nanog-GFP MEFs (NGIP MEFs), 2D4 iPS cells, and control ES cells. *Xist* (X) and *Tsix* (T) transcripts were simultaneously detected by FISH using a double-stranded DNA probe. Nuclei were counterstained with DAPI (blue). Male ES cells show the same expression pattern on the single X chromosome as female ES cells and iPS cells on both X.

(B) As in (A), except that only *Tsix* RNA was detected by using a strand-specific RNA probe.

(C) As in (B), except that only *Xist* RNA was detected by using a strand-specific RNA probe. It should be noted that directly labeled, double- (A) or single- (C) stranded FISH probes only detect *Xist* RNA when the RNA is coating the X chromosome, but not when *Xist* is expressed at low levels as seen in undifferentiated ES cells.

(D) RT-PCR analysis of *Xite* intergenic transcripts in iPS cell line 2D4, NGIP MEFs, and male control ES cells. Transcripts at different locations along the *Xite* locus were detected (regions 5–7). Positive control, *Rrm2*, a house keeping gene. Like female ES cells, male ES cells express *Xite* transcripts.

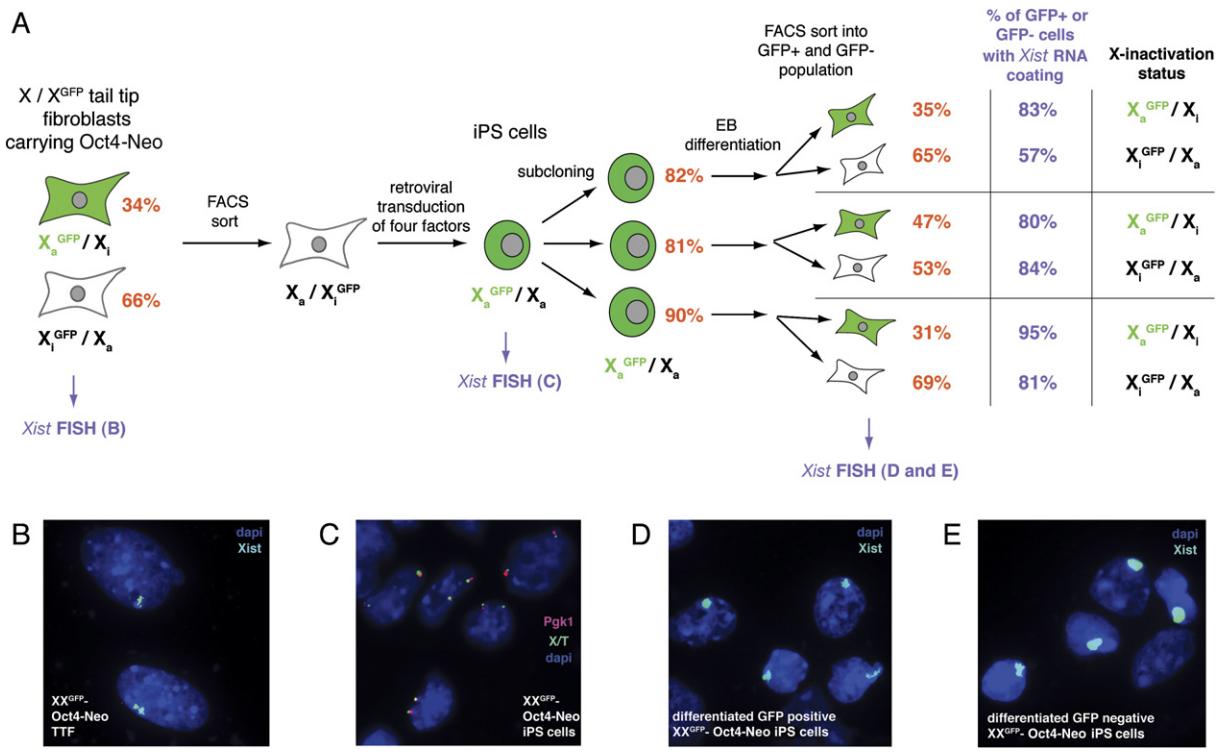

Figure 6. Random X Inactivation in Differentiating TTF-Derived iPS Cells

(A) Flow scheme for obtaining iPS cells from X^{GFP}/X TTFs and for subsequent analysis of X inactivation. X^{GFP}/X TTFs carrying the Oct4-Neo allele were sorted at two consecutive passages to obtain a GFP-negative population (Xi^{GFP}/Xa; <0.05% green cells). Reprogrammed cells were selected based on ES cell morphology and GFP reactivation. Drug selection with G418 was employed to retrospectively verify the reprogrammed state of the iPS cells, but not to select for iPS cell establishment. iPS cells were subcloned, differentiated, and analyzed by FACS and *Xist* FISH. Numbers of GFP+ or GFP− cells determined by FACS are given in orange, and the numbers given in blue indicate the percentage of cells with *Xist* RNA coating of the Xi within GFP+ and GFP− differentiated iPS cells, respectively.

(B) Localization and expression of *Xist* RNA on the Xi in the nuclei of female X^{GFP}/X TTFs of (A). *Xist* transcripts were detected by using a single-stranded RNA probe. Nuclei were counterstained with DAPI (blue).

(C) Localization and expression of *Xist*, *Tsix*, and *pgk1* RNA in the nuclei of iPS cells described in (A). *Xist* (X) and *Tsix* (T) transcripts were simultaneously detected by using a double-stranded DNA probe.

(D) As in (B), except that only GFP+ differentiated iPS cells were analyzed for *Xist* pattern.

(E) As in (B), except that only GFP− differentiated iPS cells were analyzed for *Xist* pattern.

isolated that, upon replating, were also found to be resistant to G418, thus indicating activation of the Oct4 locus in addition to reactivation of the silent X chromosome. An ES cell-like pattern of *Xist* and *Tsix* expression confirmed X reactivation (Figures 6C).

Given that these female iPS cells, like ES cells, had a tendency to lose an X chromosome when maintained continuously in culture, we subcloned Xa^{GFP}/Xa iPS cells to ensure that pure clonal populations of iPS cells were analyzed for randomness of X inactivation. Differentiation of subclones was induced by embryoid body formation, and differentiated cells were sorted by FACS into GFP-positive and GFP-negative populations and analyzed by FISH (Figure 6A). Consistent with a random pattern of X inactivation, on average 38% of the cells were GFP positive and 62% of the cells were GFP negative, and the majority of both populations had an *Xist* signal consistent with *Xist* RNA coating of the Xi (Figures 6D and 6E). Random X

(E) Immunostaining to demonstrate the nuclear pattern of H3me3K27, its methyltransferase Ezh2, and H4me1K20, in NGIP MEFs and 2D4 iPS cells. The cells were stained with the respective antibodies, and nuclei were counterstained with DAPI. The percentage of cells with an Xi-like enrichment of the respective chromatin mark is given.

(F) Detection of *Xist* RNA in differentiating 2D4 iPS cells. *Xist* FISH with a stand-specific RNA probe in undifferentiated iPS cells and iPS cells at day 4 of retinoic acid-induced differentiation.

(G) Exclusion of RNA polymerase II (Pol II) from the *Xist* RNA-coated X chromosome indicates silencing of the X in differentiating 2D4 iPS cells. 2D4 iPS cells differentiated for 5 days by retinoic acid treatment were costained for Pol II and *Xist* RNA. Nuclei were detected by DAPI.

(I) Enrichment of Ezh2 and H3me3K27 on the Xi in differentiating 2D4 iPS. The graphs show the percentage of cells with *Xist* RNA coating that show colocalization with Ezh2 or H3me3K27 on the Xi at different time points during retinoic acid-induced differentiation of 2D4 iPS cells (n > 100 for each time point).

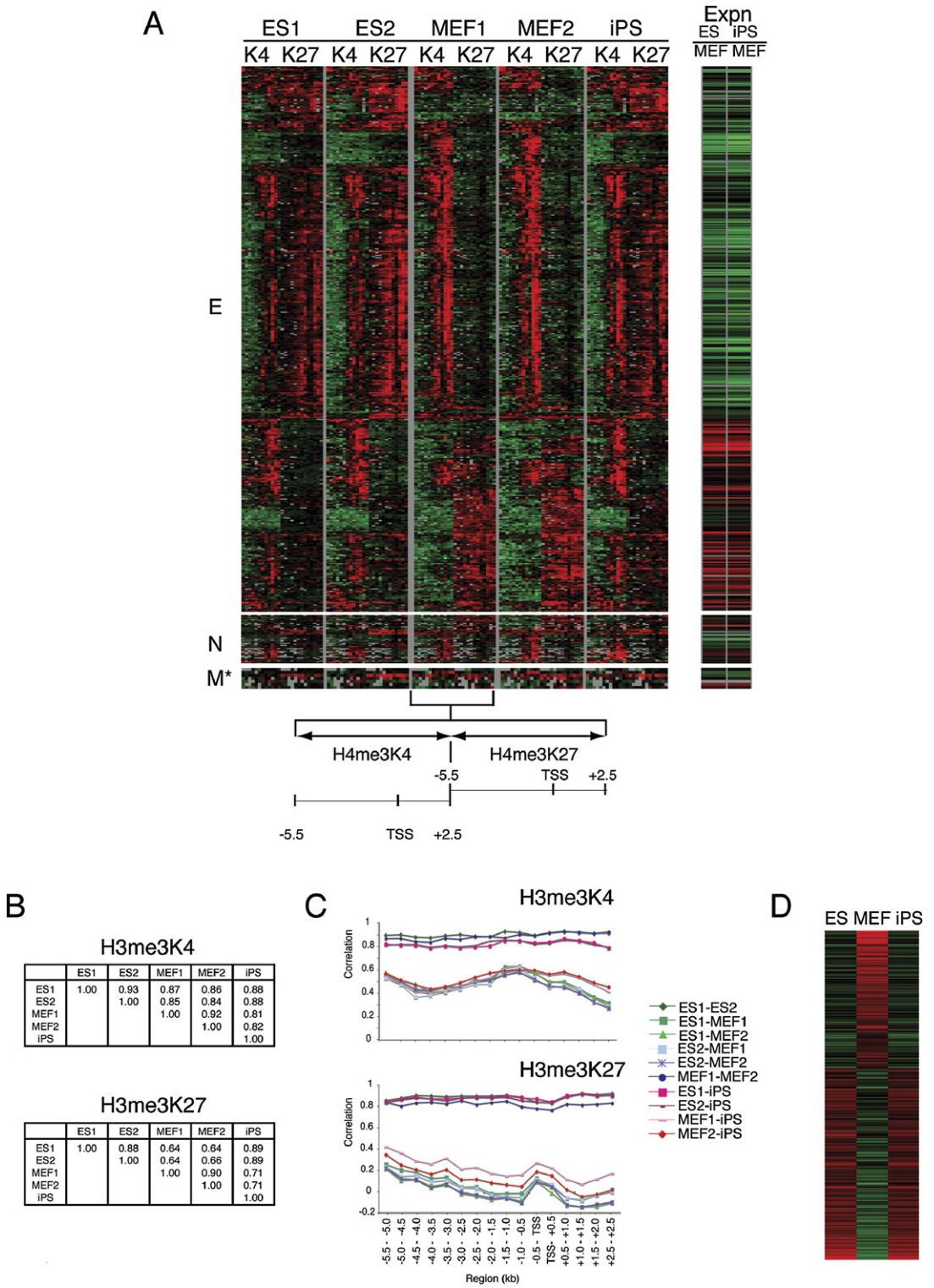

Figure 7. Global Analysis of H3K4 and H3K27 Trimethylation in iPS Cells

(A) Histone methylation pattern of 2D4 iPS cells resembles that of ES cells. Treeview representation of the hierarchical clustering of K4 and K27 methylation patterns at signature genes ($p = 0.01$) in wild-type V6.5 (ES1) and E14 (ES2) cells, male and female MEFs (MEF1 and 2, respectively), and 2D4 iPS cells. Depending on the similarity of the methylation patterns, genes were classified as E (ES-like, 903 genes), M (MEF-like, 7 genes), or N (neutral, 47 genes). E and N class genes are depicted to scale on the y axis, and the asterisk indicates that M genes are scaled 5-fold in y direction to make the methylation pattern visible. Each row represents the −5.5 kb to +2.5 kb region (total 8 kb) with respect to the transcription start site (TSS) of a single gene, reiterated ten times in total—two times for each cell type. For each cell type, the first iteration of the 8 kb region represents the enrichment for K4

inactivation confirms that the epigenetic marks that distinguish the Xa and Xi in somatic cells can be removed upon in vitro reprogramming and reestablished on either X upon subsequent in vitro differentiation.

Global Reprogramming of Histone Methylation Patterns in iPS Cells

We next asked if, in addition to DNA demethylation of the Oct4 and Nanog promoters and the reactivation of the Xi, the entire fibroblast genome had been epigenetically reprogrammed to an ES-like state during iPS cell derivation. Histone methylation plays a crucial role in epigenetic regulation of gene expression during mammalian development. In general, transcribed genes are associated with H3K4 trimethylation (Bernstein et al., 2005; Kim et al., 2005), whereas many silenced genes are associated with H3K27 trimethylation (Boyer et al., 2006; Lee et al., 2006). Genome-wide location analysis for K4 and K27 trimethylation in the Nanog-selected 2D4 iPS line, male and female MEFs, and two male ES cell lines was performed by using chromatin immunoprecipitation (ChIP) followed by hybridization to a mouse promoter array. Probes on this array cover a region from −5.5 kb upstream to +2.5 kb downstream of the transcriptional start sites for about 16,500 genes. To determine if the 2D4 iPS line was more similar to ES cells or to MEFs, we first defined a set of genes that was significantly different in the histone methylation pattern between ES cells and MEFs. At high stringency ($p = 0.01$), 957 genes were identified as being different between ES cells and MEFs and classified as "signature" genes (see Experimental Procedures). Remarkably, in 2D4 iPS cells, 94.4% of the signature genes carried a methylation pattern virtually identical to ES cells (E class genes), whereas only 0.7% of the genes were methylated in a more MEF-like pattern (M class genes). The remaining 4.9% of the loci were classified as N class genes (neutral), as the differences were too small to be significant (Figure 7A). The majority (91%) of the iPS loci remained in the E class even when the stringency was lowered to $p = 0.05$ to include a larger set of signature genes (Figure S4). The distribution into E, M, and N genes is highly significant as confirmed by a random permutation test (Figure S5). Genes that belonged to the nonsignature class showed little or no difference in methylation pattern between MEFs, ES cells, and iPS cells (data not shown), indicating that the iPS line had not acquired a completely novel epigenetic identity found neither in ES cells nor MEFs. Collectively, our results indicate that in vitro reprogramming can reverse the epigenetic memory of a fibroblast genome into one highly similar to that of ES cells.

In an effort to determine if K4 and K27 methylation patterns were reset to different extents during reprogramming, Pearson correlation was calculated separately for each methylation mark for all 16,500 genes on the array (Figure 7B). This analysis revealed that iPS cells and ES cells were as similar in their K27 methylation pattern as the two ES lines to each other, whereas MEFs clearly differed to the same extent from both iPS and ES cells. Interestingly, K4 methylation was more similar between all cell types, suggesting that reprogramming is mainly associated with changes in K27 rather than K4 trimethylation. One prediction from this global analysis is that the change in K27 methylation should be prominent in the E class of signature genes. To test this, we performed a pair-wise correlation analysis between all possible cell types at 500 bp intervals along the 8 kb promoter region, resulting in 16 correlation values for each comparison (Figure 7C). Genes classified as E genes were indeed very similar in their K4 and K27 methylation patterns between ES cells and 2D4 iPS cells along the entire analyzed region, whereas MEFs differed dramatically from both cell types throughout. In further agreement with the global correlation, K27 methylation differed more dramatically between MEFs and ES/iPS cells than K4 methylation. Based on the previous observation that developmental genes are the most important target group of PcG-mediated K27 methylation in murine ES cells (Boyer et al., 2006), we decided to test if these loci are enriched within signature genes. Indeed, gene ontology analysis revealed that developmental genes are the most significantly enriched gene group in the E class of signature genes ($p = 8 \times e^{-10}$). These findings suggested that changes in K27 methylation are more significant for the reprogramming from MEFs into iPS cells than changes in K4 methylation and suggest an important role for PcG proteins in reprogramming.

To test if the correlation of the iPS and ES cell histone methylation patterns faithfully captures changes in the transcriptional status of the iPS cells, we performed expression analysis on ES cells, 2D4 iPS cells, and MEFs at the whole-genome level with Agilent microarrays. ES and iPS cells showed a very high correlation in expression patterns at the global level as determined by Pearson correlation (Figures S6A and S6B). Genes with a more than 2-fold difference in expression between ES cells and MEFs were almost identically expressed between

and the second for the K27 trimethylation. As indicated in the schematic below, the 8 kb regions are divided into 16 colored 500 bp fragments displaying the average log ratio of the probe signal intensity for the respective fragment. Green, red, and gray represent lower-than-average, higher-than-average, and missing values for enrichment (due to the lack of probes), respectively. Expn ES/MEF and iPS/MEF depict the gene expression ratios between ES cells and MEFs and iPS cells and MEFs, respectively, with red representing higher expression and green lower expression in MEFs as compared to ES cells or reprogrammed cells.

(B) Global correlation of K4 and K27 trimethylation data between all cell types. The table shows the binary global correlation of K4 and K27 trimethylation, respectively, between all possible pairs of cell types and for all genes on the array (~16,500).

(C) Correlation of K4 and K27 trimethylation within E class genes between all cell types. Correlation values for K4 or K27 methylation for each two pairs of cell types were plotted as a function of the distance from the transcription start site in increments of 500 bp.

(D) The transcriptome of the iPS cells is reprogrammed to an ES-like state. Expression pattern of genes that show a 2-fold difference in transcript levels between ES cells and MEFs are plotted for ES cells, MEFs, and iPS cells (total 2473 genes).

ES and iPS cells (Figure 7D). Therefore, our data indicate that iPS cells, as expected from the epigenetic data, are transcriptionally highly comparable to ES cells. We next confirmed the levels of a randomly chosen subset of 13 signature genes by real-time RT-PCR (Figure S6C). All tested genes were expressed at similar levels in iPS cells and ES cells. The differences in expression of signature genes between ES, iPS cells, and MEFs correlated well with the observed differences in the histone methylation patterns (Figure 7A and Figure S6D), suggesting that K4 and K27 methylation are important determinants of the expression state of those genes. Taken together, these data demonstrate that nuclear reprogramming by four transcription factors can induce global transcriptional and epigenetic resetting of the fibroblast genome.

MEF and TTF-Derived iPS Cells Differentiate into Numerous Cell Types, Including Germ Cells

We reasoned that the faithful epigenetic reprogramming of iPS cells should result in a developmental potential that is comparable to that of ES cells. Injection of GFP-marked MEF-derived 2D4 iPS cells into diploid blastocysts gave rise to three newborn chimeras with obvious GFP fluorescence (Figure 8A and Table S2). Tissue sections from a newborn pup showed broad and clonal contribution of iPS cells to the cartilage, glandular structures, liver, heart, and lungs (Figure 8B). FACS analysis of hematopoietic cells derived from a newborn pup revealed that between 18% and 28% of splenic B cells and macrophages as well as thymic CD4+ and CD8+ T cells were derived from iPS cells (Figure 8C). Moreover, we were able to isolate iPS cell-derived tail fibroblasts and neurosphere cultures from this chimeric pup, which showed similar growth rates and cytokine dependence compared with host-derived fibroblasts and neurospheres (data not shown). One chimera that developed into adulthood showed coat color chimerism, indicating differentiation of iPS cells into functional melanocytes (Figure 8D).

We next asked if, in addition to MEF-derived iPS cells, female TTF-derived iPS cells could also support development. Blastocyst injection of two different iPS clones that had been selected based on the re-expression of an Xi^{GFP} transgene gave rise to one postnatal animal per line (Table S2 and data not shown). The chimeric animals appeared healthy and grew normally into adult mice. These results indicate that iPS cells derived from TTFs, like iPS cells derived from fetal fibroblasts, give rise to normal appearing postnatal chimeras.

Germline transmission is considered one of the most stringent tests for the pluripotency of cells. To assess whether Xi^{GFP}/X TTF-derived iPS cells can contribute to the germline, we isolated 16 oocytes from one superovulated iPS chimera, of which four were brightly GFP positive, indicating contribution of iPS cells to the female germline (Figure 8E). Treatment of these oocytes with strontium chloride and cytochalasin B resulted in successful parthenogenetic activation and subsequent cleavage to the blastocyst stage, thus demonstrating functionality of oocytes (Figure 8E).

Directed differentiation of ES cells into mature cell types has clear therapeutic potential. To determine whether iPS cells could give rise to mature cells in vitro, we generated EBs that were explanted in culture to induce hematopoietic cell fates. We indeed detected cell types expressing markers of immature and mature blood cells, thus underscoring the potential use of iPS cells in regenerative medicine (Figure S7).

DISCUSSION

The generation of pluripotent cells directly from fibroblast cultures has represented a major advance toward understanding the mechanisms that govern nuclear reprogramming (Takahashi and Yamanaka, 2006). Here, we provide evidence that faithful epigenetic resetting of the genome accompanies transcription factor-induced reprogramming. We recovered iPS cells that were remarkably similar to ES cells in their epigenome. For example, female iPS cells showed proper demethylation at the promoters of key pluripotency genes, they reactivated a somatically silenced X chromosome that underwent random X inactivation upon differentiation, and they had a global histone methylation pattern that was almost identical to that of ES cells. iPS cells also revealed other ES-like qualities, including growth factor responsiveness, the ability to act as reprogramming donors in cell fusion, as well as the ability to undergo ES-like differentiation both in vitro and in vivo, contributing to high-grade postnatal chimeras, including one germline chimera.

Our finding that transgenic Oct4 expression is not required for the maintenance of iPS cells indicates that the endogenous gene expression program has been sufficiently reactivated to ensure maintenance of pluripotency. This suggests that exogenous expression of Oct4 and possibly also that of Sox2, c-Myc, and Klf4 may only be necessary during the initial steps of reprogramming to trigger transcriptional and epigenetic changes that lead to pluripotency. In support of this notion, retroviral expression of the four factors was high in infected donor fibroblasts and silenced in iPS cells. Thus, it should be feasible to transiently supply somatic cells with the four factors, generating stably reprogrammed cells that do not contain retroviral or transgenic elements, which may result in insertional mutagenesis or gene expression artifacts, respectively.

Surprisingly, Nanog-selected iPS cells were phenotypically and molecularly different from the previously reported Fbx15-selected iPS cells. Nanog is essential for embryonic development and is required for the maintenance of pluripotency by suppressing differentiation into primitive endoderm (Chambers et al., 2003; Mitsui et al., 2003). Fbx15, in contrast, is not essential for pluripotency or development despite its exclusive expression in ES cells (Tokuzawa et al., 2003). There are several possible explanations for the qualitative differences between Fbx15-selected iPS cells and the iPS cells described in this manuscript. One possibility is that Nanog selection

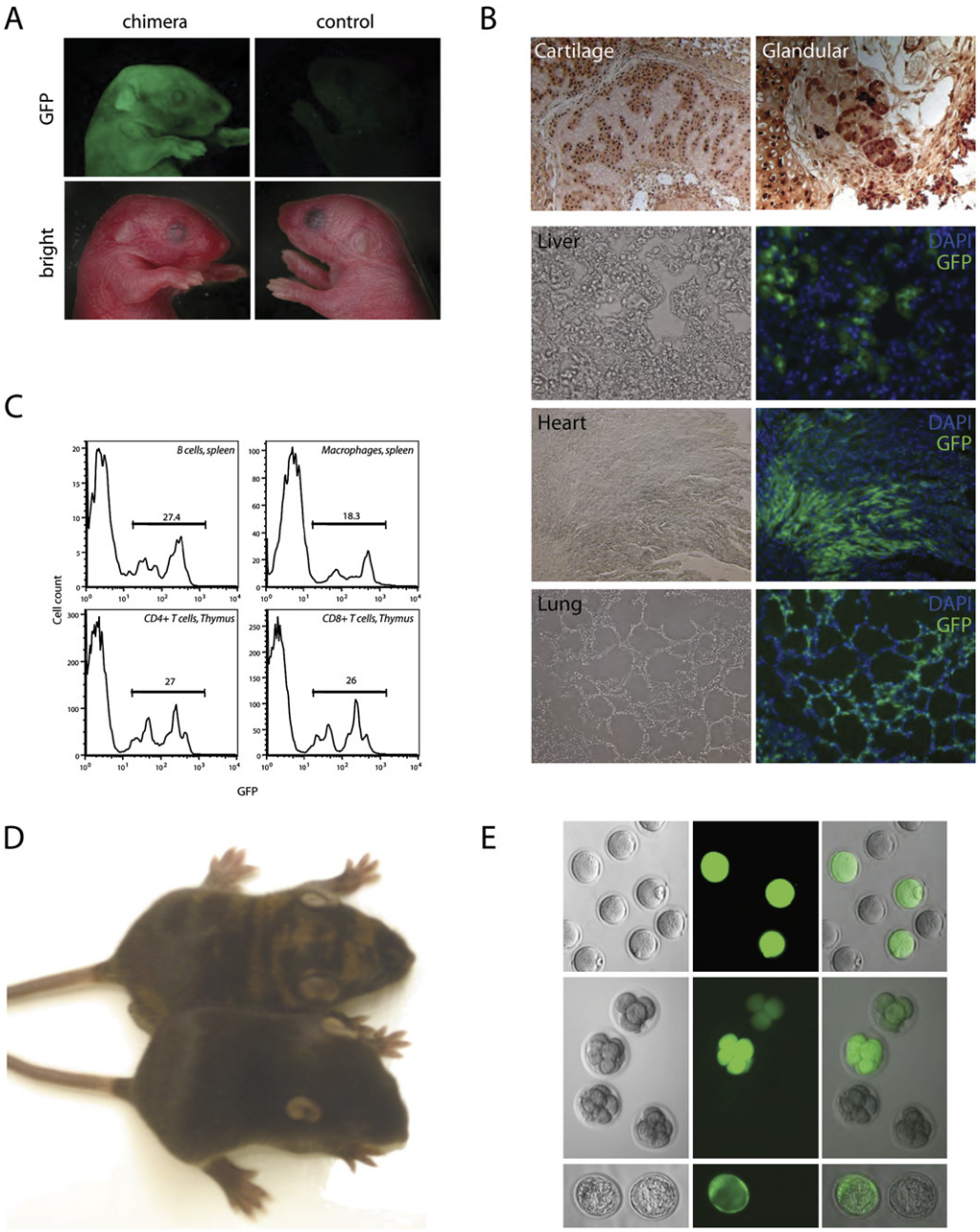

Figure 8. In Vivo Developmental Potential of Nanog-Selectable iPS Cells

(A) Cells from iPS line 2D4 that carried a randomly integrated GFP transgene were injected into blastocysts. Surrogate mothers gave birth to GFP-positive pups. A nonchimeric pup not expressing GFP is shown.

(B) Analysis of tissues from a newborn 2D4 iPS cell-derived chimera. GFP staining of paraffin sections from pups in (A) shows clonal contribution to cartilage and glandular structures (upper panels). Analysis of frozen sections of individual organs shows broad contribution of iPS-derived cells to liver, heart, and lung.

(C) Flow cytometric analysis of hematopoietic cells isolated from the spleen and thymus of a newborn iPS cell-derived chimeric mouse. Histograms denote the percentage of GFP-positive cells in populations gated on lineage-specific markers.

(D) Ten-day-old chimeric mouse derived from blastocyst-injected 2D4 iPS cells, shown next to a wild-type littermate. iPS-derived cells are responsible for the agouti coat color.

(E) Germline contribution in chimeras of female X^{GFP}/X TTF-derived iPS cells. Green oocytes indicate that iPS cells contributed to the germline (top panel). Parthenogenetic activation induces cleavage divisions into 4/8 cell-stage embryos (middle panel) and blastocysts (bottom). Shown are brightfield images, GFP images, and combined brightfield/GFP images.

gives rise to a different pluripotent cell type with greater developmental potential compared with Fbx15 selection. In agreement, most Fbx15-selected iPS cells did not express Nanog (Takahashi and Yamanaka, 2006), which may explain why they inappropriately differentiated in the absence of MEFs and failed to give rise to full-term chimeras. In further support of this notion is the observation that not all Oct4 expressing cells are also positive for Nanog in normal ES cell cultures, suggesting heterogeneity within the ES cell population (Hatano et al., 2005). Interestingly, inner cell mass cells of the blastocyst, from which ES cells are derived, show a similarly heterogeneous expression pattern for Oct4 and Nanog (Chazaud et al., 2006).

An alternative explanation for the effect of Nanog selection on the quality of resultant iPS cells could be that Nanog protein itself plays a critical role in faithful epigenetic reprogramming. In agreement with this idea, cell-fusion experiments between ES cells and somatic cells have shown to result in 200-fold more colonies when Nanog is overexpressed in ES cells (Silva et al., 2006). Although Nanog is not required for inducing pluripotency in somatic cells, it should be informative to assess whether its overexpression during the reprogramming process enhances the efficiency of obtaining iPS cells and if it affects the developmental potency of iPS cells.

Yet another possibility for the observed differences between the previously reported iPS cells and our iPS cells may be the timing of selection. We were unable to derive iPS cells from Nanog-GFP MEFs when selection was applied 3 days after infection, which is in contrast to the findings by Yamanaka and colleagues (Takahashi and Yamanaka, 2006), who were able to select for Fbx15 expression at this time. We hence started selection 1 week after infection or isolated iPS cells solely based on ES cell morphology or the reactivation of a silenced X-linked GFP transgene, followed by retrospective verification of pluripotency using the Oct4-Neo allele. All iPS cells derived without initial drug selection appeared better than the previously reported Fbx15-selected iPS cells in terms of chimeric contribution and ES cell-like epigenetic features. We hypothesize that reprogramming is a gradual process that takes several days or weeks and depends on a cascade of genes that need to be reactivated as also suggested by Wernig et al. (2007). In this scenario, Nanog reactivation might occur later during nuclear reprogramming than Fbx15 reactivation. Thus, early selection for Fbx15 may expand a cell population that has not completed nuclear reprogramming, consequently eliminating potentially better reprogrammed cells that would appear later during the reprogramming process; late selection for Nanog may capture a stage at which reprogramming is more complete. It should be interesting to test whether late selection for Fbx15 expression generates iPS cells that are more similar to ES cells. Our observation that morphological selection of ES-like colonies instead of drug selection may be sufficient for obtaining iPS cells has important implications for direct reprogramming attempts in humans, as introducing reporter transgenes into human cells is technically challenging and may cause insertional mutagenesis.

Direct reprogramming of cells to pluripotency has clear therapeutic implications, and it has therefore been crucial to ascertain whether iPS cells exist in the same epigenetic state as ES cells. Our data indicate that abnormal epigenetic reprogramming should not compromise the therapeutic utility of directly reprogrammed cells. It will undoubtedly be important to recapitulate direct reprogramming in human cells.

EXPERIMENTAL PROCEDURES

Derivation of Fibroblasts

The Nanog-GFP-iresPuro construct (Hatano et al., 2005) was targeted into male V6.5 ES cells, correctly targeted clones were confirmed by standard Southern blot analysis, and mice were generated. The Oct4-neomycin (Oct4-neo) resistance construct and resultant "knockin" mice will be described elsewhere (Wernig et al., 2007). Oct4-neomycin/hygromycin-selectable MEFs were obtained from intercrosses between Oct4-Neo mice with pgk-Hygromycin (Hygro) mice. TTFs carrying the X^{GFP} and the Oct4-Neo allele were obtained from intercrosses between Oct4-Neo and X-linked GFP mice (Hadjantonakis et al., 1998). Inducible Oct4 mice have been described previously (Hochedlinger et al., 2005). MEFs were derived from embryos at embryonic day 14.5, and TTFs from up to 1-week-old mice.

Retrovirus Production and Infection of MEFs

cDNAs for Oct4, Sox2, c-MYC (T58A mutant), and Klf4 were cloned into the retroviral pMX vector and transfected into PlatE packaging cell line (Morita et al., 2000) by using Fugene (Roche). At 48 hr posttransfection, viral supernatants were used to infect target MEFs cultured in ES media. Two to three rounds of overnight infection were performed, and cells were split onto a layer of irradiated feeders after 7 days and selected with 1 μg/mL puromycin (Sigma) or 300 μg/mL G418 (Roche) at indicated times.

Cell Culture and In Vitro Differentiation

iPS cells and ES cells were grown on irradiated murine embryonic fibroblasts (feeders) and in standard ES media (DMEM supplemented with 15% FBS, nonessential amino acids, L-glutamine, penicillin-streptomycin, β-mercaptoethanol, and with 1000 U/mL LIF). To label the 2D4 iPS cells for blastocyst injections, cells were electroporated with a Rosa-GFP-Neo targeting vector and verified by Southern blot analysis. To generate subclones from X^{GFP}/X Oct4-Neo iPS cells, cells were electroporated with a linearized pgk-Hygro plasmid. Selection was initiated 24 hr postpulse with G418 (300 μg/mL) or hygromycin (140 μg/mL), respectively. To study the state of the X chromosome, iPS cells were passaged once in ES media onto gelatin-coated dishes to reduce the number of feeder cells, and differentiation was induced with 40 ng/ml all-trans retinoic acid in ES media lacking LIF. To analyze randomness of X inactivation, differentiation was induced upon EB formation.

To isolate oocytes, the female chimera was superovulated with PMS and hCG and oocytes were isolated 13 hr after the hCG injection. To induce parthenogenetic activation, oocytes were incubated in calcium-free CZB media supplemented with 10 mM strontium chloride and 5 $\mu g/ml^{-1}$ cytochalasin B for 5 hr followed by cultivation in KSOM media at 37°C, 5% CO_2.

Southern Blot Analysis for Global DNA Methylation

Ten micrograms of genomic DNA was digested with HpaII or MspI, and fragments were separated on a 0.8% agarose gel. DNA was blotted

onto HybondXL membrane (Amersham Biosciences) and hybridized with the pMR150 probe as previously described (Meissner et al., 2005).

Bisulfite Sequencing

Bisulfite treatment of DNA was performed with the EpiTect Bisulfite Kit (Qiagen) according to manufacturer's instructions. Primer sequences were as previously described for Oct4 (Blelloch et al., 2006) and Nanog (Takahashi and Yamanaka, 2006). Amplified products were purified by using gel filtration columns, cloned into the pCR2.1-TOPO vector (Invitrogen), and sequenced with M13 forward and reverse primers.

RT-PCR Analysis

To test expression of pluripotency genes from the endogenous locus, total RNA was treated with the DNA-free Kit (Ambion, Austin, TX) and reverse transcribed with SuperScript First-Strand Synthesis System (Invitrogen) using oligo dT primers according to manufacturer instructions. All primer sequences are given in Table S3.

Western Analysis, Immuno-, and AP Staining

Antibodies are listed in Table S3. Alkaline phosphatase staining was performed with the Vector Red substrate kit (Vector Labs). Immunostaining was done according to Plath et al. (2003).

FISH Analysis

FISH was performed as described previously (Panning et al., 1997). *Xist*, *Tsix*, and *pgk1* double-stranded DNA probes were generated by random priming using Cy3-dUTP (PerkinElmer) or FITC-dUTP (Amersham) and Bioprime kit reagents (Invitrogen) from an *Xist* cDNA template and a genomic clone containing 17 kb of *pgk1* sequences, respectively. Strand-specific RNA probes to specifically detect either *Tsix* and *Xist* were generated by in vitro transcription in the presence of FITC UTP from *Xist* exon 1 and exon 6 templates. When immunofluoresence was followed by FISH, cells were fixed with 4% PFA before the FISH procedure started, and the blocking buffer contained 1 mg/ml tRNA and RNase inhibitor.

Cell Fusion

Four million iPS cells were combined with four million MEFs and fused with PEG-1500 (Roche) according to the manufacturer's directions. Selection was initiated 24 hr postfusion with puromycin (1 μg/mL) and hygromycin (140 μg/mL). For experiments involving Neo selection, G418 was used at 300 μg/mL. Cell-cycle analysis was performed on a FACSCalibur (BD) with propidium iodide; signal area was used as a measure of DNA content.

ChIP and Microarray Hybridization

Genome-wide chromatin analysis ChIP was performed with about one million cells following the protocol on http://www.upstate.com (see the Supplemental Experimental Procedures for a more detailed description). Ten nanograms of each immuoprecipitated sample and corresponding inputs were amplified with the Whole Genome Amplification Kit (Sigma), and 2 μg of amplified material was labeled with Cy3 or Cy5 (PerkinElmer) using the Bioprime Kit (Invitrogen). Hybridization onto the mouse promoter array (Agilent –G4490), washing, and scanning were carried out according to the manufacturer's instructions. Probe signals (log ratio) were extracted with the Feature extraction software, normalized with Lowess normalization of the Chip Analytics software, and statistically analyzed as described in the Supplemental Experimental Procedures.

Whole-Genome Expression Analysis

Duplicate samples of 500 ng of RNA from V6.5 ES cells, female NGiP MEFs, puromycin-selected 2D4 iPS cells, and puromycin-selected control NGiP ES cells were amplified and labeled with Cy3 using the Agilent low RNA amplification and one color labeling kit according to manufacturer's instructions. Labeled RNA was hybridized to the Agilent Mouse whole-genome array (G4122F) and analyzed as described in the Supplemental Experimental Procedures.

Flow Cytometry

For chimera analysis, spleen, thymus, and bone marrow were isolated as previously described (Ye et al., 2003); cells stained with antibodies listed in Table S3 were analyzed by FACS. Oct4-Neo X^{GFP}/X TTFs were sorted at two consecutive passages and reanalyzed to verify a pure GFP-negative population. Upon EB differentiation, cells were sorted into GFP+/GFP− populations and used for FISH analysis. Cells were acquired on a BD FACS ARIA (BD Pharmingen), and data were analyzed with FlowJo software (Tree Star, Inc.).

Teratoma Formation

Two million cells for each line were injected subcutaneously into the dorsal flank of isoflurane-anesthetized SCID mice. Teratomas were recovered 3–4 weeks postinjection, fixed overnight in 10% formalin, paraffin embedded, and processed with hematoxylin and eosin or with specific antibodies.

Histology and Immunohistochemical Analysis of GFP Expression in Chimeric Mice

Frozen sections were generated by subsequently incubating tissues in 4% PFA and 20% sucrose, followed by embedding in OCT compound and sectioning on a cryostat (10 μm thickness). Sections were coverslipped with Vectashield mounting media and DAPI and then visualized directly for GFP signal. Immunohistochemical staining for GFP was done on paraffin sections with antibody ab290-50 (Abcam).

Supplemental Data

Supplemental Data include Supplemental Experimental Procedures, seven figures, and five tables and can be found with this article online at http://www.cellstemcell.com/cgi/content/full/1/1/55/DC1/.

ACKNOWLEDGMENTS

We thank Chad Cowan, Siavash Kurdistani, Laurie Jackson-Grusby, Jeannie Lee, and Hanno Hock for critically reading the manuscript; Takashi Tada for the Nanog-GFPiresPuro construct; Toshio Kitamura for pMXs retroviral constructs and Plat-E cells; Scott Lowe for c-MYC cDNA; and Rebecca Chan for Klf4 cDNA. We also especially thank Siavash Kurdistani for advice with the microarray data analysis and Laura Prickett for help with FACS analysis. N.M. is supported by a graduate scholarship from the Natural Sciences and Engineering Council of Canada and a Sir James Lougheed Award. J.U. is supported by the Dr. Mildred Scheel Foundation for Cancer Research. K.P. is supported by the Margaret E. Early Trust Foundation and is a Special Fellow of the Leukemia and Lymphoma Society. K.H. is supported by the Harvard Stem Cell Institute and is a V Scholar.

Received: March 31, 2007
Revised: May 4, 2007
Accepted: May 14, 2007
Published: June 6, 2007

REFERENCES

Bernstein, B.E., Kamal, M., Lindblad-Toh, K., Bekiranov, S., Bailey, D.K., Huebert, D.J., McMahon, S., Karlsson, E.K., Kulbokas, E.J., 3rd, Gingeras, T.R., et al. (2005). Genomic maps and comparative analysis of histone modifications in human and mouse. Cell *120*, 169–181.

Blelloch, R., Wang, Z., Meissner, A., Pollard, S., Smith, A., and Jaenisch, R. (2006). Reprogramming efficiency following somatic cell nuclear transfer is influenced by the differentiation and methylation state of the donor nucleus. Stem Cells *24*, 2007–2013.

Boyer, L.A., Plath, K., Zeitlinger, J., Brambrink, T., Medeiros, L.A., Lee, T.I., Levine, S.S., Wernig, M., Tajonar, A., Ray, M.K., et al. (2006). Polycomb complexes repress developmental regulators in murine embryonic stem cells. Nature *441*, 349–353.

Chambers, I., Colby, D., Robertson, M., Nichols, J., Lee, S., Tweedie, S., and Smith, A. (2003). Functional expression cloning of Nanog, a pluripotency sustaining factor in embryonic stem cells. Cell *113*, 643–655.

Chazaud, C., Yamanaka, Y., Pawson, T., and Rossant, J. (2006). Early lineage segregation between epiblast and primitive endoderm in mouse blastocysts through the Grb2-MAPK pathway. Dev. Cell *10*, 615–624.

Cowan, C.A., Atienza, J., Melton, D.A., and Eggan, K. (2005). Nuclear reprogramming of somatic cells after fusion with human embryonic stem cells. Science *309*, 1369–1373.

Eggan, K., Akutsu, H., Hochedlinger, K., Rideout, W., 3rd, Yanagimachi, R., and Jaenisch, R. (2000). Science *290*, 1578–1581.

Gaudet, F., Hodgson, J.G., Eden, A., Jackson-Grusby, L., Dausman, J., Gray, J.W., Leonhardt, H., and Jaenisch, R. (2003). Induction of tumors in mice by genomic hypomethylation. Science *300*, 489–492.

Hadjantonakis, A.K., Gertsenstein, M., Ikawa, M., Okabe, M., and Nagy, A. (1998). Non-invasive sexing of preimplantation stage mammalian embryos. Nat. Genet. *19*, 220–222.

Hatano, S.Y., Tada, M., Kimura, H., Yamaguchi, S., Kono, T., Nakano, T., Suemori, H., Nakatsuji, N., and Tada, T. (2005). Pluripotential competence of cells associated with Nanog activity. Mech. Dev. *122*, 67–79.

Heard, E. (2005). Delving into the diversity of facultative heterochromatin: the epigenetics of the inactive X chromosome. Curr. Opin. Genet. Dev. *15*, 482–489.

Hochedlinger, K., and Jaenisch, R. (2006). Nuclear reprogramming and pluripotency. Nature *441*, 1061–1067.

Hochedlinger, K., Yamada, Y., Beard, C., and Jaenisch, R. (2005). Ectopic expression of Oct-4 blocks progenitor-cell differentiation and causes dysplasia in epithelial tissues. Cell *121*, 465–477.

Kim, T.H., Barrera, L.O., Zheng, M., Qu, C., Singer, M.A., Richmond, T.A., Wu, Y., Green, R.D., and Ren, B. (2005). A high-resolution map of active promoters in the human genome. Nature *436*, 876–880.

Lee, T.I., Jenner, R.G., Boyer, L.A., Guenther, M.G., Levine, S.S., Kumar, R.M., Chevalier, B., Johnstone, S.E., Cole, M.F., Isono, K., et al. (2006). Control of developmental regulators by polycomb in human embryonic stem cells. Cell *125*, 301–313.

Meissner, A., Gnirke, A., Bell, G.W., Ramsahoye, B., Lander, E.S., and Jaenisch, R. (2005). Reduced representation bisulfite sequencing for comparative high-resolution DNA methylation analysis. Nucleic Acids Res. *33*, 5868–5877.

Mitsui, K., Tokuzawa, Y., Itoh, H., Segawa, K., Murakami, M., Takahashi, K., Maruyama, M., Maeda, M., and Yamanaka, S. (2003). The homeoprotein Nanog is required for maintenance of pluripotency in mouse epiblast and ES cells. Cell *113*, 631–642.

Morita, S., Kojima, T., and Kitamura, T. (2000). Plat-E: an efficient and stable system for transient packaging of retroviruses. Gene Ther. *7*, 1063–1066.

Ng, K., Pullirsch, D., Leeb, M., and Wutz, A. (2007). Xist and the order of silencing. EMBO Rep. *8*, 34–39.

Ogawa, Y., and Lee, J.T. (2003). Xite, X-inactivation intergenic transcription elements that regulate the probability of choice. Mol. Cell *11*, 731–743.

Panning, B., Dausman, J., and Jaenisch, R. (1997). X chromosome inactivation is mediated by Xist RNA stabilization. Cell *90*, 907–916.

Plath, K., Fang, J., Mlynarczyk-Evans, S.K., Cao, R., Worringer, K.A., Wang, H., de la Cruz, C.C., Otte, A.P., Panning, B., and Zhang, Y. (2003). Role of histone H3 lysine 27 methylation in X inactivation. Science *300*, 131–135.

Rideout, W.M., 3rd, Eggan, K., and Jaenisch, R. (2001). Nuclear cloning and epigenetic reprogramming of the genome. Science *293*, 1093–1098.

Sears, R., Nuckolls, F., Haura, E., Taya, Y., Tamai, K., and Nevins, J.R. (2000). Multiple Ras-dependent phosphorylation pathways regulate Myc protein stability. Genes Dev. *14*, 2501–2514.

Silva, J., Mak, W., Zvetkova, I., Appanah, R., Nesterova, T.B., Webster, Z., Peters, A.H., Jenuwein, T., Otte, A.P., and Brockdorff, N. (2003). Establishment of histone h3 methylation on the inactive X chromosome requires transient recruitment of Eed-Enx1 polycomb group complexes. Dev. Cell *4*, 481–495.

Silva, J., Chambers, I., Pollard, S., and Smith, A. (2006). Nanog promotes transfer of pluripotency after cell fusion. Nature *441*, 997–1001.

Tada, M., Takahama, Y., Abe, K., Nakatsuji, N., and Tada, T. (2001). Nuclear reprogramming of somatic cells by in vitro hybridization with ES cells. Curr. Biol. *11*, 1553–1558.

Takahashi, K., and Yamanaka, S. (2006). Induction of pluripotent stem cells from mouse embryonic and adult fibroblast cultures by defined factors. Cell *126*, 663–676.

Thorvaldsen, J.L., Verona, R.I., and Bartolomei, M.S. (2006). X-tra! X-tra! News from the mouse X chromosome. Dev. Biol. *298*, 344–353.

Tokuzawa, Y., Kaiho, E., Maruyama, M., Takahashi, K., Mitsui, K., Maeda, M., Niwa, H., and Yamanaka, S. (2003). Fbx15 is a novel target of Oct3/4 but is dispensable for embryonic stem cell self-renewal and mouse development. Mol. Cell. Biol. *23*, 2699–2708.

Wakayama, T., Perry, A.C., Zuccotti, M., Johnson, K.R., and Yanagimachi, R. (1998). Full-term development of mice from enucleated oocytes injected with cumulus cell nuclei. Nature *394*, 369–374.

Wernig, M., Meissner, A., Foreman, R., Brambrink, T., Ku, M., Hochedlinger, K., Bernstein, B.E., and Jaenisch, R. (2007). In vitro reprogramming of fibroblasts into a pluripotent ES cell-like state. Nature, in press.

Wilmut, I., Schnieke, A.E., McWhir, J., Kind, A.J., and Campbell, K.H. (1997). Viable offspring derived from fetal and adult mammalian cells. Nature *385*, 810–813.

Ye, M., Iwasaki, H., Laiosa, C.V., Stadtfeld, M., Xie, H., Heck, S., Clausen, B., Akashi, K., and Graf, T. (2003). Hematopoietic stem cells expressing the myeloid lysozyme gene retain long-term, multilineage repopulation potential. Immunity *19*, 689–699.

Zvetkova, I., Apedaile, A., Ramsahoye, B., Mermoud, J.E., Crompton, L.A., John, R., Feil, R., and Brockdorff, N. (2005). Global hypomethylation of the genome in XX embryonic stem cells. Nat. Genet. *37*, 1274–1279.

Accession Numbers

Microarray data have been deposited under the GEO accession number GSE7815.